Displacement and stress convergence of our MITC plate bending elements

Klaus-Jürgen Bathe and Miguel Luiz Bucalem
Department of Mechanical Engineering, Massachusetts Institute of Technology, Cambridge, Massachusetts 02139, USA

and Franco Brezzi
Dipartimento di Meccanica Strutturale and Istituto di Analisi Numerica del CNR, 27100 Pavia, Italy
(Received July 1990)

ABSTRACT

We briefly summarize the theoretical formulations of our MITC plate bending elements and then present numerical convergence results. The elements are based on Reissner–Mindlin plate theory and a mixed-interpolation of the transverse displacement, section rotations and transverse shear strain components. We consider our 4, 9 and 16-node quadrilateral elements and our 7 and 12-node triangular elements. The theoretical and numerical results indicate the high reliability and effectiveness of our elements.

INTRODUCTION

The development of finite elements for the analysis of plate and shell structures has been a very active area of research over the past two decades. The current state-of-the-art in plate and shell analyses has been given by Noor *et al.*[1].

We presented a review[2] of our thoughts towards shell element research and an approach for formulating general shell elements that are reliable and effective. There, and in our earlier works[3,4], we stated that the aim in our element developments is to satisfy (among others) the following important two conditions:

- An element should be mechanistically clear and 'numerically sound': it must not contain any spurious zero energy mode, it must not ever lock and must not be based on numerically adjusted factors.
- The predictive capability of the element should be high and be relatively insensitive to element geometric distortions.

Many elements proposed in the literature for plate and shell analysis violate these conditions to a high degree, and while they may provide interesting research results, such elements are not yet useful in engineering practice and require further development.

A very promising approach towards the development of general plate and shell elements has been the use of an isoparametric formulation. However, considering the formulation of isoparametric plate and shell elements (degenerate from three-dimensional conditions or equivalently, for plate analysis, based on Reissner–Mindlin plate theory), the only pure displacement-based element that can be recommended for general practical analysis of plates/shells is the 16-node bicubic element with 4×4 Gauss integration[3]. However, while reliable and in some analyses efficient, the element can exhibit a rather low convergence rate when geometrically distorted elements are used. This is largely due to the effects of membrane and shear locking that are negligible when the element is flat and undistorted but increase in the element as it becomes increasingly geometrically distorted—a most undesirable phenomenon.

To establish reliable and efficient lower-order elements, and improve the performance of the 16-node element, we have concentrated our research efforts on the use of the interpolation of displacements and strain components. Correspondingly, we call the elements that we have developed the MITC elements: they are based on Mixed-Interpolated Tensorial Components.

In references 2, 5 and 6 we proposed the MITC4 and MITC8 shell elements. The construction of these elements was based on insight into element behaviour and the use of the patch test. However, we endeavoured to place the formulation approach onto a rigorous mathematical foundation[7]. The resulting mathematical analyses led to some interesting and quite general results for the linear analysis of plates, *and* we identified additional MITC elements for the plate bending problem[8–10]. Since these new plate bending elements are constructed much like the MITC4 and MITC8 elements, we can develop these elements with the approach of reference 2—and are currently doing so—also for general shell analysis.

We should note here also that during recent years a number of other researchers have taken similar approaches towards plate element formulations[1,11], but our plate elements contain some differences and have a good mathematical foundation.

The objective in this paper is to briefly summarize the construction of our MITC elements for the plate

0264–4401/90/040291-12$2.00

bending problem and give some numerical convergence results. The elements considered are the MITC4, MITC9 and MITC16 quadrilateral elements and the MITC7 and MITC12 triangular elements. Additional MITC elements were proposed by Brezzi *et al.*[10] and additional theoretical and numerical results are given in earlier papers[2,5-9,12].

PLATE BENDING PROBLEM AND OUR DISCRETIZATION

We consider the sequence of problems P_t in which the thickness t goes to zero and the load has the form $t^3 p(x_1, x_2)$ per unit mid-surface area with $p(x_1, x_2)$ given and fixed. A typical problem of this sequence has then the form:

$$\min_{\theta, w} \left\{ \frac{t^3}{2} a(\theta, \theta) + \frac{\lambda t}{2} \int_\Omega |\theta - \nabla w|^2 \, d\Omega - t^3 \int_\Omega pw \, d\Omega \right\} \tag{1}$$

which divided by t^3 becomes:

$$\min_{\theta, w} \left\{ \frac{1}{2} a(\theta, \theta) + \frac{\lambda t^{-2}}{2} \int_\Omega |\theta - \nabla w|^2 \, d\Omega - \int_\Omega pw \, d\Omega \right\} \tag{2}$$

Here $(t^3/2)a(\theta, \theta)$ is the bending internal energy and $(\lambda t/2)\int_\Omega |\theta - \nabla w|^2 \, d\Omega$ is the shear energy [3].

A finite element is effective if the solution to any problem in the sequence (uniformly in t) yields good approximations. We presented[7] a detailed analysis of our MITC4 element for the solution of (2).

However, a simplified test on whether an element is effective was proposed[8]: since we are interested in the limit behaviour for $t \to 0$ we might restrict ourselves to the limit problem $t = 0$. It is clear that if an element is uniformly good for $t \to 0$ it will also be good for $t = 0$, but the converse is not necessarily true. Intuitively the test $(t = 0)$ makes sense and as can be seen[7,12] the test is indeed very useful. Hence we can concentrate on the limit problem of (2), which can be written as:

$$\min_{\substack{\theta, w \\ \theta = \nabla w}} \left\{ \frac{1}{2} a(\theta, \theta) - \int_\Omega pw \, d\Omega \right\} \tag{3}$$

The members of the family of elements that we are going to discuss here are constructed like the MITC4 and MITC8 elements[2,5]. In particular we have to choose: (i) a finite element space $\mathbf{\Theta}_h$ for the approximation of the rotations, (ii) a finite element space W_h for the approximation of the transverse displacement, (iii) a finite element space $\mathbf{\Gamma}_h$ for the approximation of the shear strains and, finally, (iv) a 'reduction operator' R_h which interpolates piecewise smooth functions into $\mathbf{\Gamma}_h$.

Accordingly the discrete version of (2) becomes:

$$\min_{\theta_h, w_h} \left\{ \frac{1}{2} a(\theta_h, \theta_h) + \frac{\lambda t^{-2}}{2} \int_\Omega |R_h(\theta_h - \nabla w_h)|^2 \, d\Omega - \int_\Omega pw_h \, d\Omega \right\} \tag{4}$$

and the corresponding limit problem $(t = 0)$ is:

$$\min_{\substack{\theta_h, w_h \\ R_h(\theta_h - \nabla w_h) = 0}} \left\{ \frac{1}{2} a(\theta_h, \theta_h) - \int_\Omega pw_h \, d\Omega \right\} \tag{5}$$

The aim is now to find choices for $\mathbf{\Theta}_h$, W_h, $\mathbf{\Gamma}_h$ and R_h such that (5) has a unique solution which converges, as the mesh parameter $h \to 0$, to the solution of (3) with optimal error bounds.

The construction of the appropriate choices starts by recognizing that for every pair θ, w with

$$\theta = \nabla w \tag{6}$$

of smooth functions, we want to find a corresponding pair $\theta^I \in \mathbf{\Theta}_h$ and $w^I \in W_h$ with

$$R_h(\theta^I - \nabla w^I) = \mathbf{0} \tag{7}$$

which approximates (θ, w) with optimal error bounds. It is clear that, if this can be done (and if R_h is a good approximation of the identity, as you expect from a decent interpolation operator) then the minimum of a quadratic functional (as is $\frac{1}{2}a(\theta, \theta) - \int_\Omega pw \, d\Omega$) over the set of pairs satisfying (7) will be a good approximation to the minimum of the same functional over the set of pairs satisfying (6).

The first step of the element formulation is therefore to find θ^I and w^I. Our crucial assumption for the function $w_h \in W_h$ is that:

$$R_h(\nabla w_h) = \nabla w_h \qquad \forall w_h \in W_h \tag{8}$$

so that (7) becomes:

$$R_h \theta^I = \nabla w^I \tag{9}$$

Now, by setting for a general vector valued function ϕ,

$$\operatorname{rot} \phi = \frac{\partial \phi_2}{\partial x_1} - \frac{\partial \phi_1}{\partial x_2}$$

we recognize that a necessary condition for (9) to hold is that:

$$\operatorname{rot}(R_h \theta^I) = 0 \tag{10}$$

Since the rot operator is formally very close to the divergence operator, we are facing a situation very similar to the one that is encountered in the solution of the Stokes problem of incompressible fluids. There (for the Stokes problem) we have a smooth function $\mathbf{u}$ with div $\mathbf{u}=0$, and want to find a finite element approximation $\mathbf{u}_h$ which satisfies div $\mathbf{u}_h=0$. Such finite element approximation must be judiciously constructed, and much attention has been focused on this task. Consequently, we can find in the literature[13] many pairs $(\mathbf{U}_h, P_h)$ of velocity–pressure approximations such that the discretization of the Stokes problem:

find $\mathbf{u}_h \in \mathbf{U}_h$ and $p_h \in P_h$ such that

$$\left.\begin{aligned} &\int_\Omega \nabla \mathbf{u}_h : \nabla \mathbf{v}_h \, d\Omega - \int_\Omega p_h \operatorname{div} \mathbf{v}_h \, d\Omega \\ &\qquad = \int_\Omega \mathbf{f} \cdot \mathbf{v}_h \, d\Omega, \qquad \forall \mathbf{v}_h \in \mathbf{U}_h \\ &\int_\Omega q_h \operatorname{div} \mathbf{u}_h \, d\Omega = 0, \qquad \forall q_h \in P_h \end{aligned}\right\} \tag{11}$$

is well-posed, stable and has optimal convergence properties to the continuous solution. A sufficient condition for that is the inf–sup condition:

$$\exists \beta > 0 \text{ such that } \inf_{q_h \in P_h} \sup_{v_h \in \mathbf{U}_h} \frac{\int_\Omega q_h \operatorname{div} \mathbf{v}_h \, d\Omega}{\|q_h\|_{L^2} \|\mathbf{v}_h\|_{H^1}} \geqslant \beta \tag{12}$$

With this example in mind, we try something similar. For a given $\boldsymbol{\theta} = \nabla w$ smooth, we look for $\boldsymbol{\theta}^I$ as the discrete solution of:

find $(\boldsymbol{\theta}^I, q^I)$ in $(\boldsymbol{\Theta}_h, Q_h)$ such that

$$\left.\begin{aligned} &\int_\Omega \nabla \boldsymbol{\theta}^I : \nabla \boldsymbol{\eta}_h \, d\Omega - \int_\Omega q^I \operatorname{rot} \boldsymbol{\eta}_h \, d\Omega \\ &\qquad = \int_\Omega \nabla \boldsymbol{\theta} : \nabla \boldsymbol{\eta}_h \, d\Omega, \qquad \forall \boldsymbol{\eta}_h \in \boldsymbol{\Theta}_h \\ &\int_\Omega q_h \operatorname{rot} \boldsymbol{\theta}^I \, d\Omega = 0, \qquad \forall q_h \in Q_h \end{aligned}\right\} \tag{13}$$

In (13), $\boldsymbol{\Theta}_h$ is the finite element space that we are going to choose for the approximation of rotations while Q_h is an auxiliary 'pressure space' that will never enter the Reissner–Mindlin plate element formulation (it is not present in (4)). Hence our first step is the choice of a pair of finite element spaces $\boldsymbol{\Theta}_h$, Q_h such that:

$$\exists \beta > 0 \text{ such that } \inf_{q_h \in Q_h} \sup_{\boldsymbol{\eta}_h \in \boldsymbol{\Theta}_h} \frac{\int_\Omega q_h \operatorname{rot} \boldsymbol{\eta}_h \, d\Omega}{\|q_h\|_{L^2} \|\boldsymbol{\eta}_h\|_{H^1}} \geqslant \beta \tag{14}$$

In perfect analogy with what is done for the Stokes problem (11), it is now easy to see that if (14) holds true, problem (13) has a unique solution $\boldsymbol{\theta}^I$, q^I and that $\boldsymbol{\theta}^I \to \boldsymbol{\theta}$, $q^I \to 0$ (with optimal order) as $h \to 0$. We discard q^I (we have no use for it) and keep the precious $\boldsymbol{\theta}^I$. On our way to (9) we have reached an intermediate step: we constructed a $\boldsymbol{\theta}^I$ in $\boldsymbol{\Theta}_h$, close to $\boldsymbol{\theta}$ and satisfying:

$$\int_\Omega q_h \operatorname{rot} \boldsymbol{\theta}^I \, d\Omega = 0 \quad \text{for all} \quad q_h \in Q_h \tag{15}$$

We have now to choose the reduction operator R_h together with its 'arrival space' $\boldsymbol{\Gamma}_h$. We want R_h (and $\boldsymbol{\Gamma}_h$) to be such that (15) implies (10). This will surely be true if the following diagram:

$$\begin{array}{ccc} (H_0^1)^2 & \xrightarrow{\text{rot}} & L^2 \\ R_h \downarrow & & \downarrow \pi_h \\ \boldsymbol{\Gamma}_h & \xrightarrow{\text{rot}} & Q_h \end{array} \tag{16}$$

commutes. In (16) π_h is the orthogonal projection (in $L^2(\Omega)$) into Q_h. Note that (16) implies in particular that, for every γ_h in $\boldsymbol{\Gamma}_h$ we have rot $\gamma_h \in Q_h$. Note also that (15) can be written as:

$$\pi_h(\operatorname{rot} \boldsymbol{\theta}^I) = 0 \tag{17}$$

If the diagram (16) commutes, then we have

$$\operatorname{rot}(R_h \boldsymbol{\theta}^I) = \pi_h(\operatorname{rot} \boldsymbol{\theta}^I) \tag{18}$$

and (17), (18) imply the desired (10). Hence our second step is to choose R_h and $\boldsymbol{\Gamma}_h$ in such a way that (16) commutes. On the other hand (16) (or rather its analogue with 'div' instead of 'rot') is *the* crucial step in the approximation of linear elliptic problems with mixed methods and we can easily find in the literature (e.g Ref. 13) many choices of triplets $(\boldsymbol{\Gamma}_h, Q_h, R_h)$ which are convenient. Note the special role of the auxiliary space Q_h: it never enters the actual computations but it is the only *link* between our first step (choice of $\boldsymbol{\Theta}_h$ and Q_h satisfying (14)) and our second step (choice of $\boldsymbol{\Gamma}_h, Q_h, R_h$ satisfying (16)).

Now that we have (10), we can start looking for w^I. As we have seen, if the domain is simply connected, (10) implies that $R_h \boldsymbol{\theta}^I$ is the gradient of some function: we want this function to belong to W_h. This condition, together with assumption (8), completely characterizes W_h. Actually we must have

$$\nabla W_h = \{\gamma_h \in \boldsymbol{\Gamma}_h \text{ such that } \operatorname{rot} \gamma_h = 0\} \tag{19}$$

In other words, (19) tells us that we have no more freedom in the choice of W_h. On the other hand, if (19) holds, then (10) will imply the existence of a $w^I \in W_h$ such that:

$$R_h \boldsymbol{\theta}^I = \nabla w^I \tag{20}$$

that is (9). If moreover (as is always the case in practice) R_h is a good approximation of the identity, then we have

$$\nabla w^I = R_h \theta^I \simeq \theta^I \simeq \theta = \nabla w \tag{21}$$

and w^I will be a good approximation of w.

Let us finally summarize the three basic steps of our element construction:

1st Step. Choose $\mathbf{\Theta}_h$, Q_h so that (14) holds.
2nd Step. Choose $\mathbf{\Gamma}_h$, R_h such that (16) commutes.
3rd Step. Choose W_h according to (19).

Remark As can be seen, in the construction of θ^I we discarded the 'pressure part' q^I of the solution of (13). Hence what is really only needed is that (13) produces a good 'velocity' θ^I; specifically, if the discretization produces spurious checkerboard modes in the variable q^I, this will not be a difficulty as long as θ^I is a good approximation of θ. In a sense, then, (14) is too strong, since it ensures good stability and accuracy *both* for θ^I and q^I. Some attractive choices of finite elements for the Stokes problem (as the widely used bilinear velocities/constant pressure ($Q_1 - P_0$) element) are known to produce good results for velocities and poor results for pressures (see Reference 14 for a proof of this observation in some particular cases), and it follows that the plate bending complements of such elements should not be discarded *a priori* (for example, the MITC4 element being the plate bending complement of the $Q_1 - P_0$ element provides very good results).

In the following section we summarize the elements that we find attractive and for which we present numerical convergence studies later.

MITC ELEMENTS

The MITC element formulations comprise the choice of the spaces $\mathbf{\Theta}_h$, W_h, $\mathbf{\Gamma}_h$ and the tying used, as expressed by R_h, between the interpolations in $\mathbf{\Gamma}_h$ and the transverse shear strain components as evaluated from $\mathbf{\Theta}_h$ and W_h.

We present below the choices for each element considered using the Cartesian coordinates x, y, thus considering uniform rectangular and triangular decompositions. The same interpolations are used in natural coordinates for the covariant strain components in general elements[2,5,6,9].

Regarding the notation, we have used in previous works the superscript I (e.g. MITC9^I in Reference 9) to indicate that an integral-tying for the transverse shear strains was enforced when also a point-tying could be used. Since we use in this paper always the integral-tying, we drop the superscript I.

MITC4 element

For the 4-node element we use[5,6]:

$$\mathbf{\Theta}_h = \{\boldsymbol{\eta} \mid \boldsymbol{\eta} \in (H_0^1(\Omega))^2,\ \boldsymbol{\eta}|_K \in (Q_1)^2\ \forall K\} \tag{22}$$

$$W_h = \{\zeta \mid \zeta \in H_0^1(\Omega),\ \zeta|_K \in Q_1\ \forall K\} \tag{23}$$

where Q_1 is the set of polynomials of degree $\leqslant 1$ in each variable and K is the current element in the discretization. The space $\mathbf{\Gamma}_h$ is given by:

$$\mathbf{\Gamma}_h = \{\boldsymbol{\delta} \mid \boldsymbol{\delta}|_K \in TR(K)\ \forall K,\ \boldsymbol{\delta}\cdot\boldsymbol{\tau} \text{ continuous at the interelement boundaries}\} \tag{24}$$

where $\boldsymbol{\tau}$ is the tangential unit vector to each edge of the element and

$$TR(K) = \{\boldsymbol{\delta} \mid \delta_1 = a_1 + b_1 y,\ \delta_2 = a_2 + b_2 x\} \tag{25}$$

The space $TR(K)$ is a sort of rotated Raviart–Thomas space of order zero[15]. The reduction operator R_h is given by:

$$\int_e (\boldsymbol{\eta} - R_h \boldsymbol{\eta}) \cdot \boldsymbol{\tau}\, ds = 0 \quad \text{for all edges } e \text{ of } K \tag{26}$$

This 4-node plate bending element is the complement of the 4/1 element for incompressible analysis[16] and the theoretically predicted error estimates using uniform meshes are

$$\|\theta - \theta_h\|_1 \leqslant ch \tag{27}$$

$$\|\nabla w - \nabla w_h\|_0 \leqslant ch \tag{28}$$

In (27), (28) and similar equations below, 'c' denotes a constant (different in each equation and dependent on the actual problem considered) that is independent of h, and $\|\cdot\|_0$ and $\|\cdot\|_1$ denote Sobolev norms. Specifically, for a vector valued function $\boldsymbol{\phi}$ with $\boldsymbol{\phi}^{\mathrm{T}} = [\phi_1 \phi_2]$ we have

$$\|\boldsymbol{\phi}\|_0 = \left[\int_\Omega ((\phi_1)^2 + (\phi_2)^2)\, d\Omega\right]^{1/2} \tag{29}$$

$$\|\boldsymbol{\phi}\|_1 = \left[\int_\Omega ((\phi_1)^2 + (\phi_2)^2 + (\phi_{1,1})^2 + (\phi_{1,2})^2 + (\phi_{2,1})^2 + (\phi_{2,2})^2)\, d\Omega\right]^{1/2} \tag{30}$$

Note that for this element we do not yet have theoretical convergence results available for the transverse shear strains. Some results concerning the convergence of the shear strains have recently been obtained for the following higher-order elements[12].

However, it is still not clear whether they are optimal. In general, the predicted rates in $\|\cdot\|_0$ for the shear strains of the elements below are of one order less than the corresponding rates, given below, for the rotations in the $\|\cdot\|_1$ norm.

MITC7 element

For the 7-node triangular element we use[9,10]:

$$\boldsymbol{\Theta}_h=\{\boldsymbol{\eta}\,|\,\boldsymbol{\eta}\in(H_0^1(\Omega)^2,\ \boldsymbol{\eta}|_T\in(S_7(T))^2\ \forall T\} \quad (31)$$

$$W_h=\{\zeta\,|\,\zeta\in H_0^1(\Omega),\ \zeta|_T\in P_2\ \forall T\} \quad (32)$$

where T is the triangular element in the discretization, P_2 is the space of complete second-order polynomials (corresponding to a 6-node element), and S_7 is

$$S_7(T)=\{\varphi\,|\,\varphi\in P_3,\ \varphi|_e\in P_2 \text{ on each edge } e \text{ of } T\} \quad (33)$$

where P_3 is the space of complete third-order polynomials. The space $\boldsymbol{\Gamma}_h$ is given by:

$$\boldsymbol{\Gamma}_h=\{\boldsymbol{\delta}\,|\,\boldsymbol{\delta}|_T\in TR_1(T)\ \forall T,\ \boldsymbol{\delta}\cdot\boldsymbol{\tau} \text{ continuous at the interelement boundaries}\} \quad (34)$$

where

$$TR_1(T)=\{\boldsymbol{\delta}\,|\,\delta_1=a_1+b_1x+c_1y+y(\mathrm{d}x+ey);\ \delta_2=a_2+b_2x+c_2y-x(\mathrm{d}x+ey)\} \quad (35)$$

The space $TR_1(T)$ is a kind of rotated Raviart–Thomas space of order one[15]. The reduction operator R_h is given by:

$$\int_e(\boldsymbol{\eta}-R_h\boldsymbol{\eta})\cdot\boldsymbol{\tau}p_1(s)\,\mathrm{d}s=0\ \forall e \text{ edge of } T,\ \forall p_1(s)\in P_1(e) \quad (36)$$

$$\int_T(\boldsymbol{\eta}-R_h\boldsymbol{\eta})\,\mathrm{d}x\,\mathrm{d}y=\mathbf{0} \quad (37)$$

where P_1 is the space of polynomials of degree $\leqslant 1$.

This 7-node plate bending element is the complement of the Crouzeix–Raviart element for incompressible analysis[17] and the theoretically predicted error estimates using uniform meshes are:

$$\|\boldsymbol{\theta}-\boldsymbol{\theta}_h\|_1\leqslant ch^2 \quad (38)$$

$$\|\nabla w-\nabla w_h\|_0\leqslant ch^2 \quad (39)$$

MITC9 element

For the 9-node element we use[8-10]:

$$\boldsymbol{\Theta}_h=\{\boldsymbol{\eta}\,|\,\boldsymbol{\eta}\in(H_0^1(\Omega))^2,\ \boldsymbol{\eta}|_K\in(Q_2)^2\ \forall K\} \quad (40)$$

$$W_h=\{\zeta\,|\,\zeta\in H_0^1(\Omega),\ \zeta|_K\in Q_2^r\ \forall K\} \quad (41)$$

where Q_2 is the set of polynomials of degree $\leqslant 2$ in each variable corresponding to a nine node element, and Q_2^r is the usual serendipity reduction of Q_2 corresponding to an eight node element. Note that Q_2^r can also be written as $Q_2\cap P_3$.

The space $\boldsymbol{\Gamma}_h$ is given by:

$$\boldsymbol{\Gamma}_h=\{\boldsymbol{\delta}\,|\,\boldsymbol{\delta}|_K\in G_1(K)\ \forall K,\ \boldsymbol{\delta}\cdot\boldsymbol{\tau} \text{ continuous at the interelement boundaries}\} \quad (42)$$

where

$$G_1(K)=\{\boldsymbol{\delta}\,|\,\delta_1=a_1+b_1x+c_1y+d_1xy+e_1y^2;\ \delta_2=a_2+b_2x+c_2y+d_2xy+e_2x^2\} \quad (43)$$

The space G_1 is some kind of rotated Brezzi–Douglas–Fortin–Marini space[18]. The reduction operator R_h is given by:

$$\int_e(\boldsymbol{\eta}-R_h\boldsymbol{\eta})\cdot\boldsymbol{\tau}p_1(s)\,\mathrm{d}s=0\ \forall e \text{ edge of } K,\ \forall p_1(s)\in P_1(e) \quad (44)$$

$$\int_K(\boldsymbol{\eta}-R_h\boldsymbol{\eta})\,\mathrm{d}x\,\mathrm{d}y=\mathbf{0} \quad (45)$$

This 9-node plate bending element is the complement of the 9/3 element for incompressible analysis[16] and the theoretically predicted error estimates using uniform meshes are:

$$\|\boldsymbol{\theta}-\boldsymbol{\theta}_h\|_1\leqslant ch^2 \quad (46)$$

$$\|\nabla w-\nabla w_h\|_0\leqslant ch^2 \quad (47)$$

MITC12 element

The MITC12 element is an extension of the MITC7 element. Here we use

$$\boldsymbol{\Theta}_h=\{\boldsymbol{\eta}\,|\,\boldsymbol{\eta}\in(H_0^1(\Omega))^2,\ \boldsymbol{\eta}|_T\in(S_{12}(T))^2\ \forall T\} \quad (48)$$

$$W_h=\{\zeta\,|\,\zeta\in H_0^1(\Omega),\ \zeta|_T\in P_3\ \forall T\} \quad (49)$$

where

$$S_{12}(T)=\{\varphi\,|\,\varphi\in P_4,\ \varphi|_e\in P_3 \text{ on each edge } e \text{ of } T\} \quad (50)$$

where P_4 is the space of complete fourth-order polynomials. The space $\boldsymbol{\Gamma}_h$ is given by:

$$\boldsymbol{\Gamma}_h=\{\boldsymbol{\delta}\,|\,\boldsymbol{\delta}|_T\in TR_2(T)\ \forall T,\ \boldsymbol{\delta}\cdot\boldsymbol{\tau} \text{ continuous at the interelement boundaries}\} \quad (51)$$

where

$$TR_2(T)=\{\boldsymbol{\delta}\,|\,\delta_1=a_1+b_1x+c_1y+d_1x^2+e_1xy+f_1y^2+y(gx^2+hxy+iy^2);\ \delta_2=a_2+b_2x+c_2y+d_2x^2+e_2xy+f_2y^2-x(gx^2+hxy+iy^2)\} \quad (52)$$

The space $TR_2(T)$ is a kind of rotated Raviart–Thomas space of order two[15]. The reduction operator R_h is given by:

$$\int_e (\boldsymbol{\eta}-R_h\boldsymbol{\eta})\cdot\boldsymbol{\tau}p_2(s)\,\mathrm{d}s=0\ \forall e \text{ edge of } T,\quad \forall p_2(s)\in P_2(e) \tag{53}$$

$$\int_T (\boldsymbol{\eta}-R_h\boldsymbol{\eta})\cdot\mathbf{p}_1\,\mathrm{d}x\,\mathrm{d}y=0\ \forall\mathbf{p}_1\in(P_1(T))^2 \tag{54}$$

The theoretically predicted error estimates for the MITC12 element are

$$\|\boldsymbol{\theta}-\boldsymbol{\theta}_h\|_1\leqslant ch^3 \tag{55}$$

$$\|\nabla w-\nabla w_h\|_0\leqslant ch^3 \tag{56}$$

MITC16 element

The MITC16 element is an extension of the MITC9 element. Here we use

$$\boldsymbol{\Theta}_h=\{\boldsymbol{\eta}|\ \boldsymbol{\eta}\in(H_0^1(\Omega))^2,\ \boldsymbol{\eta}|_K\in(Q_3)^2\ \forall K\} \tag{57}$$

$$W_h=\{\zeta|\ \zeta\in H_0^1(\Omega),\ \zeta|_K\in Q_3\cap P_4\ \forall K\} \tag{58}$$

where Q_3 is the space of polynomials of degree $\leqslant 3$ in each variable corresponding to a 16-node element. The space $\boldsymbol{\Gamma}_h$ is given by:

$$\boldsymbol{\Gamma}_h=\{\boldsymbol{\delta}|\ \boldsymbol{\delta}|_K\in G_2(K)\,\forall K,\ \boldsymbol{\delta}\cdot\boldsymbol{\tau} \text{ continuous at the interelement boundaries}\} \tag{59}$$

where

$$G_2(K)=\{\boldsymbol{\delta}|\ \delta_1=a_1+b_1x+c_1y+d_1x^2+e_1xy+f_1y^2+g_1x^2y+h_1xy^2+i_1y^3;\ \delta_2=a_2+b_2x+c_2y+d_2x^2+e_2xy+f_2y^2+g_2x^2y+h_2xy^2+i_2x^3\} \tag{60}$$

The space G_2 is some kind of rotated Brezzi–Douglas–Fortin–Marini space[18]. The reduction operator R_h is given by:

$$\int_e (\boldsymbol{\eta}-R_h\boldsymbol{\eta})\cdot\boldsymbol{\tau}p_2(s)\,\mathrm{d}s=0\ \forall e \text{ edge of } K,\quad \forall p_2(s)\in P_2(e) \tag{61}$$

$$\int_K (\boldsymbol{\eta}-R_h\boldsymbol{\eta})\cdot\mathbf{p}_1\,\mathrm{d}x\,\mathrm{d}y=0\ \forall\mathbf{p}_1\in(P_1(K))^2 \tag{62}$$

The theoretically predicted error estimates for the MITC16 element are:

$$\|\boldsymbol{\theta}-\boldsymbol{\theta}_h\|_1\leqslant ch^3 \tag{63}$$

$$\|\nabla w-\nabla w_h\|_0\leqslant ch^3 \tag{64}$$

NUMERICAL TESTS

We present in this section some example analyses performed with the elements of the previous section. However, before we give the results let us note:

- the element matrices are all evaluated using full numerical Gauss integration (hence no reduced integration is used),
- the elements do not contain any spurious zero energy mode,
- the elements pass the patch test, see *Figure 1* for an example solution. (Actually the MITC9 element shows a small difference to the analytical solution, but we can say that the patch test is practically passed[9].)

Convergence in the analysis of an 'ad-hoc problem'

We consider the problem of a square Reissner–Mindlin plate of side lengths two units (see *Figure 2*). The interior loading is $p=0$ and the imposed boundary displacement and section rota-

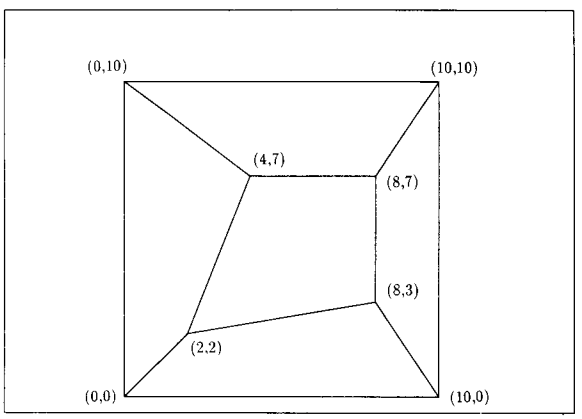

Figure 1 Patch of elements used in patch test, thickness/length = 1/1000. Support conditions correspond to only eliminating the rigid body modes. For triangular elements, one quadrilateral element is replaced by two triangular elements

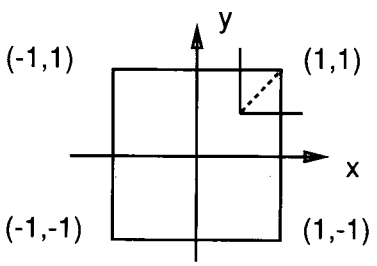

Figure 2 Square plate used in analysis of ad-hoc problem. The dashed line indicates the subdivision used for the triangular element meshes

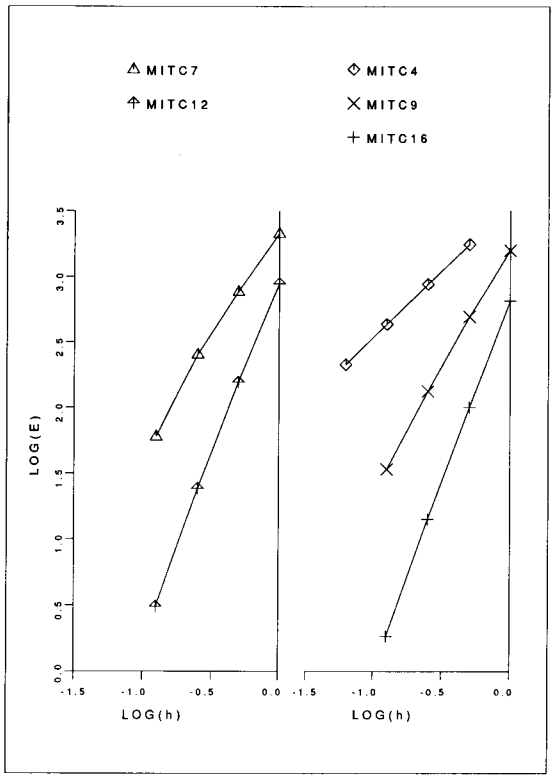

Figure 3a Convergence of section rotations in analysis of ad-hoc problem using uniform meshes. The error measure is $E=\|\boldsymbol{\theta}-\boldsymbol{\theta}_h\|_1$

tions correspond to:

$$w=\sin kx\,\mathrm{e}^{ky}+\sin k\,\mathrm{e}^{-k} \tag{65}$$

$$\theta_x=k\cos kx\,\mathrm{e}^{ky} \tag{66}$$

$$\theta_y=k\sin kx\,\mathrm{e}^{ky} \tag{67}$$

with $k=5$. We note that the above equations satisfy the Reissner–Mindlin plate equations for any value of the thickness t, and hence represent the complete (boundary and interior) solution. There is no boundary layer[19,20], and indeed the transverse shear strains are zero.

Hence this problem is a valuable test problem in that the numerically calculated convergence rates should be close to the theoretically predicted rates.

The plate problem was solved with uniform meshes, where h denotes the side length of each element.

Figure 3 shows the error in the finite element solutions in the Sobolev norms mentioned earlier, and the convergence of the transverse shear strains, and *Table 1* gives the average convergence rates. We note that the slopes of the curves in *Figure 3* are in essence constant, and hence the convergence for each element is measured to be quite uniform for each h used.

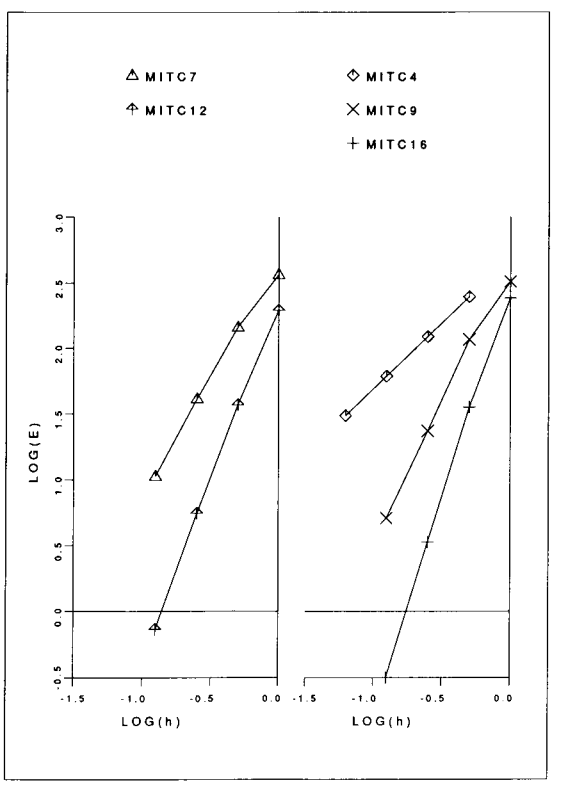

Figure 3b Convergence of gradient of vertical displacement in analysis of ad-hoc problem using uniform meshes. The error measure is $E=\|\nabla w-\nabla w_h\|_0$

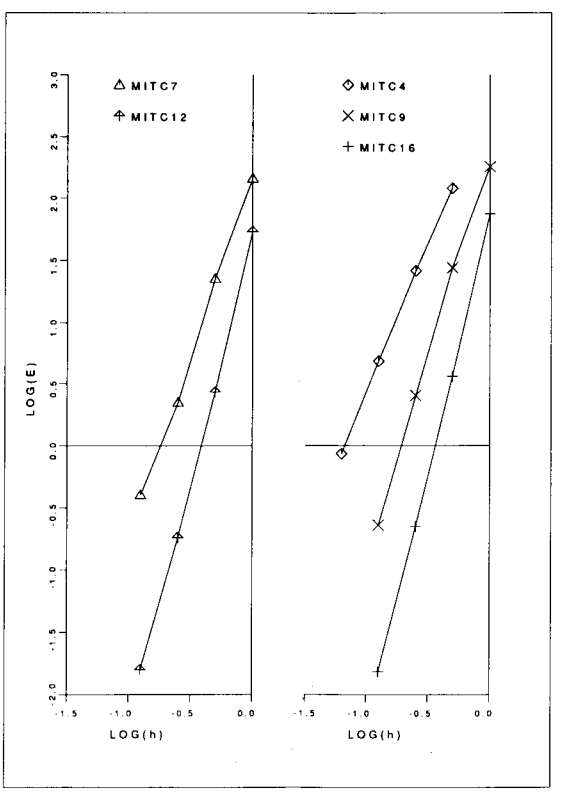

Figure 3c Convergence of transverse shear strains in analysis of ad-hoc problem using uniform meshes. The error measure is $E=\|\gamma-\gamma_h\|_0$

Table 1 Convergence rates obtained in analysis of ad-hoc problem using uniform meshes

	$\|\boldsymbol{\theta}-\boldsymbol{\theta}_h\|_1$			$\|\nabla w-\nabla w_h\|_0$			
Element	Theory	Numerical	$\|\boldsymbol{\theta}-\boldsymbol{\theta}_h\|_0$	Theory	Numerical	$\|w-w_h\|_0$	$\|\gamma-\gamma_h\|_0$
MITC4	1.0	1.0	2.0	1.0	1.0	2.1	2.4
MITC9	2.0	1.8	2.7	2.0	2.0	3.0	3.2
MITC7	2.0	1.7	2.7	2.0	1.7	2.9	2.8
MITC12	3.0	2.7	3.7	3.0	2.7	3.8	3.9
MITC16	3.0	2.8	3.7	3.0	3.2	4.2	4.1

Table 2 Convergence rates obtained in analysis of ad-hoc problem using non-uniform distorted meshes

	$\|\boldsymbol{\theta}-\boldsymbol{\theta}_h\|_1$			$\|\nabla w-\nabla w_h\|_0$			
Element	Theory	Numerical	$\|\boldsymbol{\theta}-\boldsymbol{\theta}_h\|_0$	Theory	Numerical	$\|w-w_h\|_0$	$\|\gamma-\gamma_h\|_0$
MITC4	1.0	1.0	1.9	1.0	0.8	1.7	2.3
MITC9	2.0	1.6	2.4	2.0	1.7	2.6	2.8
MITC7	2.0	1.3	2.0	2.0	1.4	2.4	2.6
MITC12	3.0	2.1	2.8	3.0	2.1	2.9	3.0
MITC16	3.0	2.4	3.2	3.0	2.4	3.2	3.1

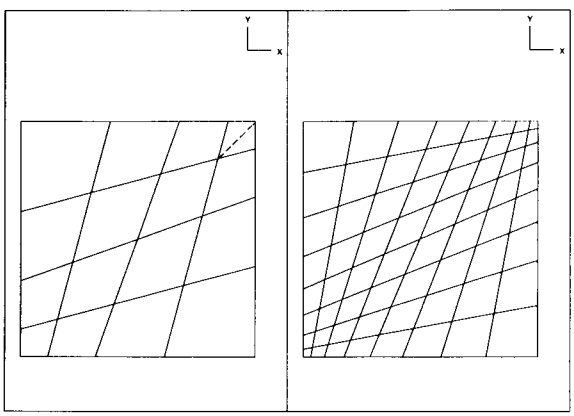

Figure 4 Two typical distorted meshes used in analysis of ad-hoc problem. -----, indicates the subdivision used for the triangular element meshes

Table 1 shows that the numerically obtained convergence rates are quite close to the theoretical rates, and that the convergence of the transverse shear strain components is surprisingly good.

In the above solutions we used uniform meshes of square elements. In a next study we deliberately distorted the elements in order to identify the effect of element distortions on the convergence rates. *Figure 4* shows the 4×4 and 8×8 element meshes used. The additional mesh refinements were obtained by similar geometric subdivisions.

Figure 5 shows the calculated errors in the solutions with the distorted meshes and *Table 2* summarizes the mean convergence rates. In *Figure 5* the element 'size' h is the corresponding element 'size' of the uniform mesh with the same number of elements.

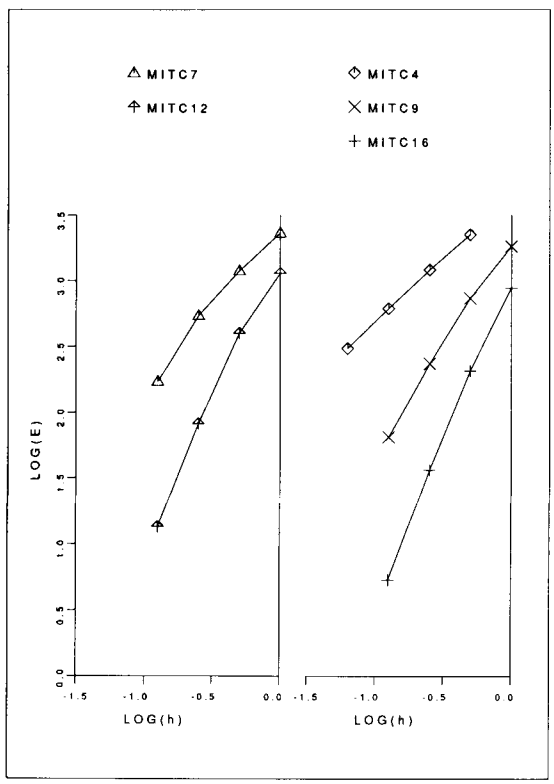

Figure 5a Convergence of section rotations in analysis of ad-hoc problem using distorted meshes. The error measure is $E=\|\boldsymbol{\theta}-\boldsymbol{\theta}_h\|_1$

A comparison of the data given in *Tables 1* and *2* shows that the use of distorted meshes results generally into a decrease of the convergence rates, but this decrease is not drastic when considering that rather highly distorted meshes were used, and when

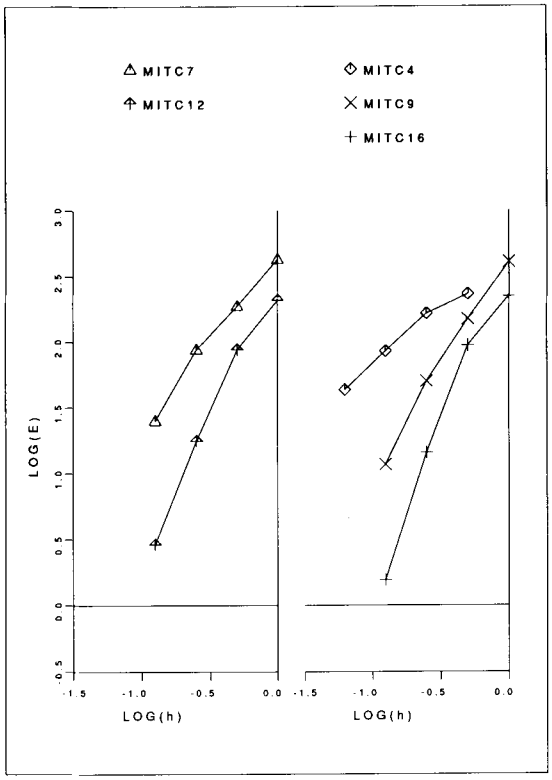

Figure 5b Convergence of gradient of vertical displacement in analysis of ad-hoc problem using distorted meshes. The error measure is $E = \|\nabla w - \nabla w_h\|_0$

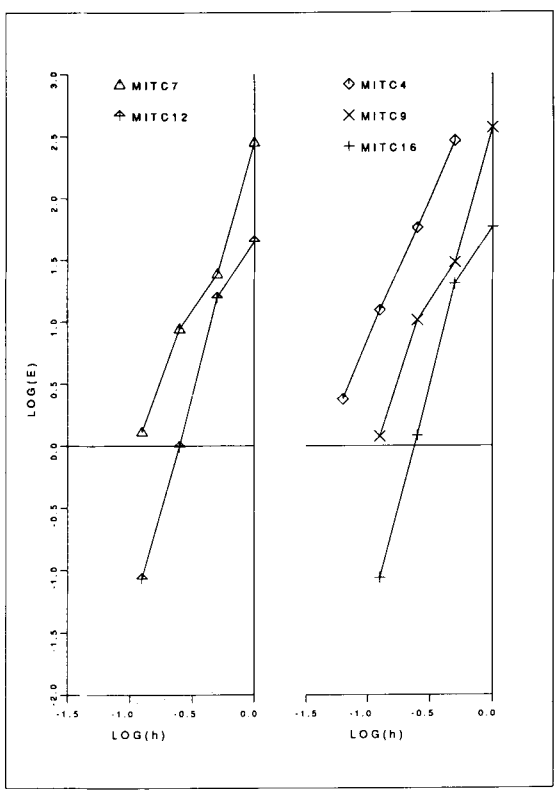

Figure 5c Convergence of transverse shear strains in analysis of ad-hoc problem using distorted meshes. The error measure is $E = \|\gamma - \gamma_h\|_0$

taking into account that each mesh contained rather large and small elements.

Convergence in the analysis of a circular plate

In this solution we consider a circular plate of thickness t and diameter D. The plate is loaded by a uniform pressure and is simply-supported or clamped along its edge.

Figure 6 gives the data of the problem considered and shows the finite element meshes used. Note that the elements are geometrically distorted in a natural way in order to model the plate.

Of particular interest in this analysis is the prediction of the transverse shear stresses. The analytical solution is rather simple (see *Figure 7*) and there is no boundary layer. *Figure 7* shows the calculated stresses as obtained for the simply-supported plate using the MITC16 element and the usual 16-node displacement-based element. In this Figure we show the stresses calculated at those nodal points along line PO where two elements meet. The stresses for an element at a nodal point have been calculated using for that element

$$\tau = \mathbf{C}\hat{\mathbf{B}}\mathbf{u} \tag{68}$$

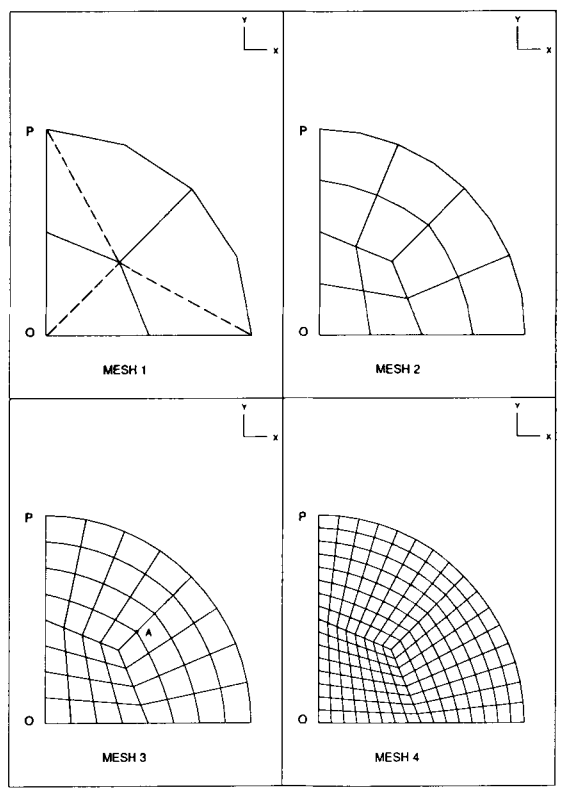

Figure 6 Finite element meshes used in analysis of circular plate. The broken line in mesh 1 indicates the subdivision used to obtain the triangular element meshes. Young's modulus $E = 2.1 \times 10^6$, Poisson's ratio $\nu = 0.3$, pressure $p = 0.03072$, diameter $D = 20.0$

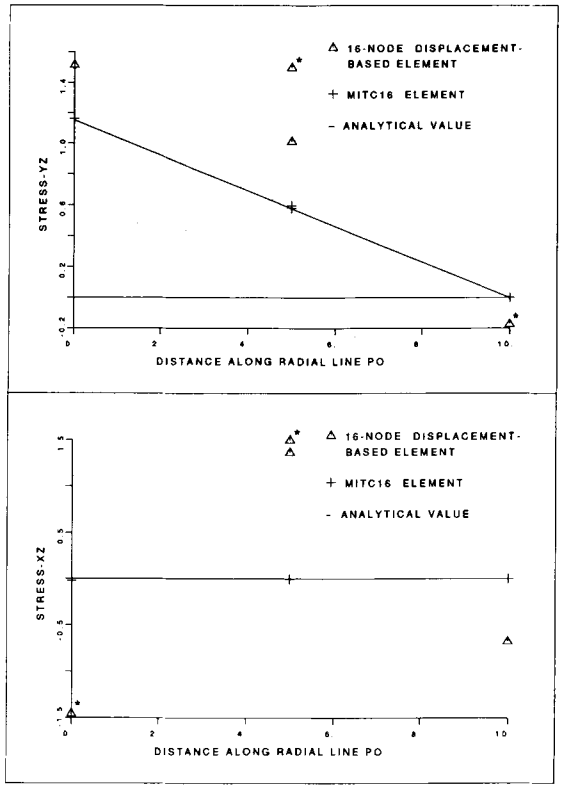

Figure 7a Transverse shear stress predictions for simply supported circular plate, $t/D=1/100$. Mesh 1 with three quadrilateral elements. For the 16-node displacement-based element the results shown with a star (*) are actually outside the Figure

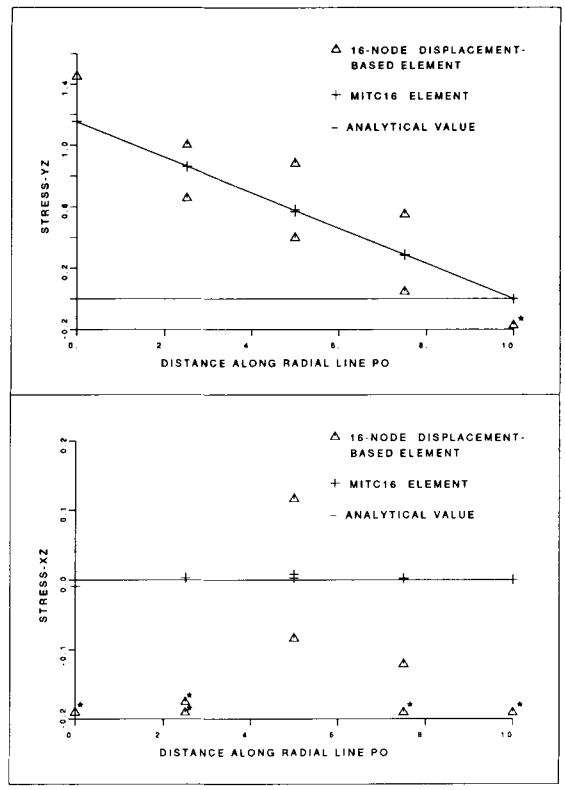

Figure 7b Transverse shear stress predictions for simply supported circular plate, $t/D=1/100$. Mesh 2 with twelve quadrilateral elements. For the 16-node displacement-based element the results shown with a star (*) are actually outside the Figure

where τ is the vector of the stresses, $\mathbf{C}$ is the stress–strain matrix, $\hat{\mathbf{B}}$ is the strain–displacement matrix of the element at the nodal point considered and $\mathbf{u}$ is the element nodal point displacement vector.

Hence there is no stress smoothing and at nodal points where elements meet in *Figure 7* two values for each shear stress component are obtained. We note that the solution is quite accurate using the MITC16 element with only three elements. On the other hand, the displacement-based element does not give an accurate transverse shear stress prediction unless a very fine mesh is employed.

In order to identify the effect of a further geometric distortion of a mesh, we also solved the problem with the mesh of *Figure 8*. The results of the transverse shear stress *yz* for the clamped plate are shown in *Figure 9*. We note that when using the MITC elements, the artificial geometric distortion does not greatly affect the accuracy in the predicted stresses.

For the calculation of the bending stress we can use mesh 2 of *Figure 6* that already gives very accurate predictions using the MITC9 and MITC16 elements. The results for the clamped plate are shown in *Figure 10* for the stresses calculated at all nodal points of each element using (68).

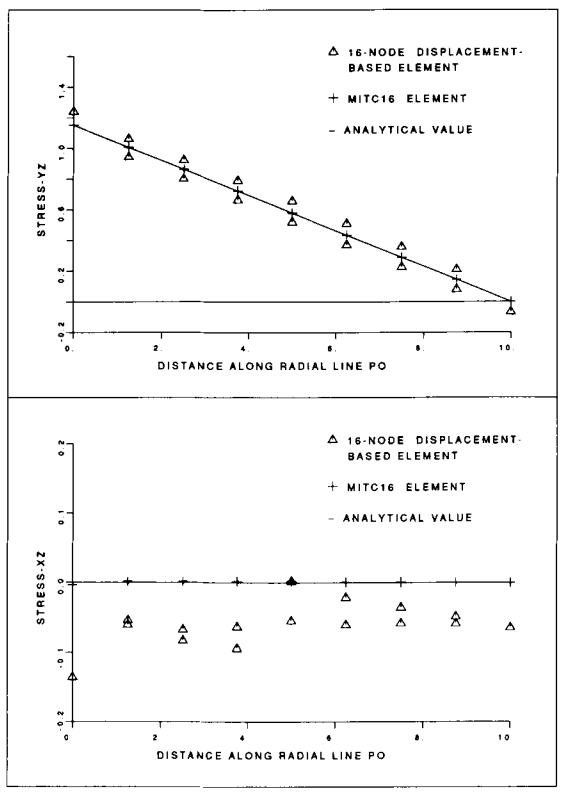

Figure 7c Transverse shear stress predictions for simply supported circular plate, $t/D=1/100$. Mesh 3 with forty-eight quadrilateral elements

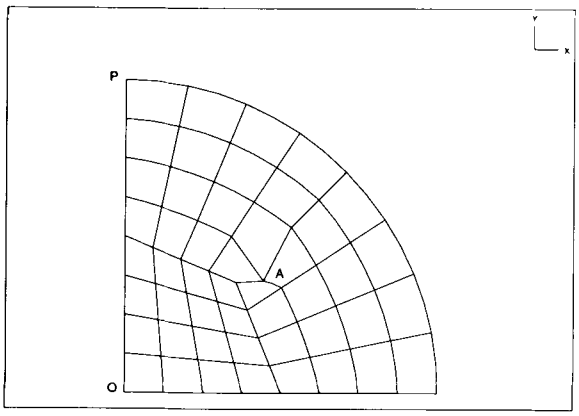

Figure 8 Artificially distorted mesh (of mesh 3) used in analysis of circular plate

Finally, we calculated the convergence rates in the solution of the problems when using the various MITC elements. *Tables 3* and *4* summarize the results. We note that in general good convergence is obtained, but the quadrilateral elements perform better than the triangular elements. This is, of course, not unusual. We may also mention that the slopes of the error curves as h is decreasing from mesh 1 to mesh 4 were in most cases quite constant but in a few cases they varied considerably from the average values given in *Tables 3* and *4*.

The Tables show a good correlation between the theoretical convergence rates and the numerically calculated rates for the quadrilateral elements, and

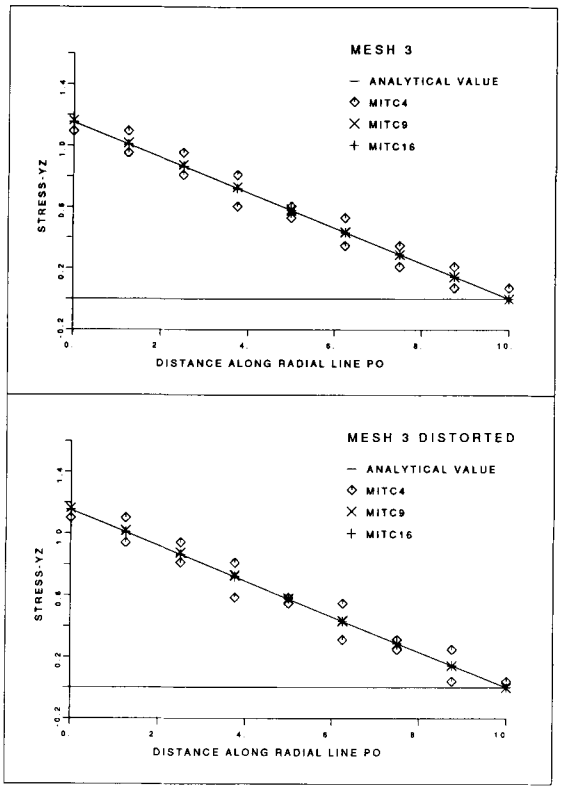

Figure 9 Transverse shear stress predictions for clamped circular plate, $t/D=1/100$

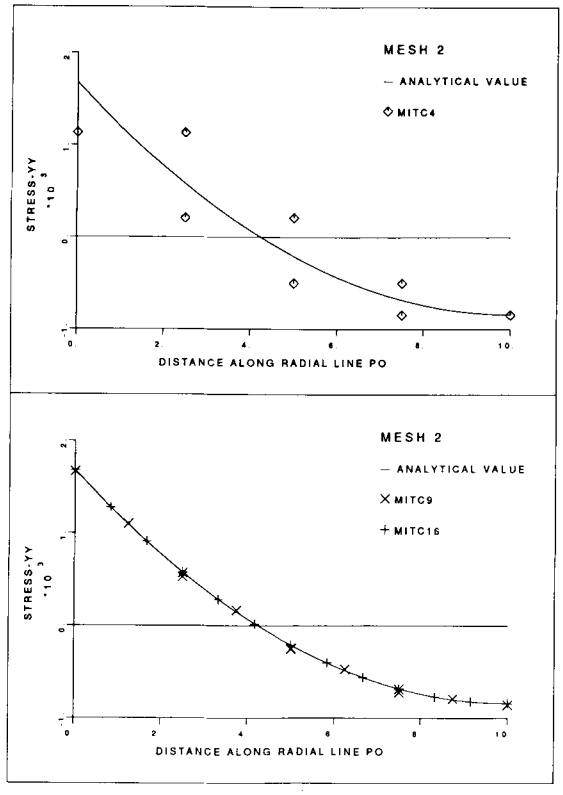

Figure 10 Radial bending stress predictions for clamped circular plate, $t/D=1/100$. The stresses calculated at all nodal points along line PO are shown

Table 3 Convergence rates obtained in analysis of clamped circular plate, $t/D=1/1000$

Element	$\|\theta-\theta_h\|_1$ Theory	$\|\theta-\theta_h\|_1$ Numerical	$\|\theta-\theta_h\|_0$	$\|\nabla w-\nabla w_h\|_0$ Theory	$\|\nabla w-\nabla w_h\|_0$ Numerical	$\|w-w_h\|_0$	$\|\gamma-\gamma_h\|_0$ $t/D=1/1000$	$\|\gamma-\gamma_h\|_0$ $t/D=1/100$
MITC4	1.0	1.2	1.9	1.0	0.8	1.9	0.94	0.95
MITC9	2.0	2.2	3.1	2.0	2.0	3.0	1.4	1.6
MITC7	2.0	1.9	2.7	2.0	1.4	2.5	0.5	1.2
MITC12	3.0	2.2	3.1	3.0	2.1	3.1	1.1	1.4
MITC16	3.0	2.9	3.8	3.0	3.4	4.5	1.6	1.9

Table 4 Convergence rates obtained in analysis of simply supported circular plate, $t/D=1/1000$

	$\|\theta-\theta_h\|_1$			$\|\nabla w-\nabla w_h\|_0$			$\|\gamma-\gamma_h\|_0$	
Element	Theory	Numerical	$\|\theta-\theta_h\|_0$	Theory	Numerical	$\|w-w_h\|_0$	$t/D=1/1000$	$t/D=1/100$
MITC4	1.0	1.4	1.9	1.0	1.0	1.9	0.95	0.96
MITC9	2.0	2.0	2.9	2.0	2.0	3.1	0.7	1.8
MITC7	2.0	1.4	2.0	2.0	1.1	2.1	0.3	1.1
MITC12	3.0	2.1	2.9	3.0	2.1	3.2	1.5	1.6
MITC16	3.0	2.8	3.7	3.0	3.3	4.5	1.2	2.0

they show an overall robustness of the MITC4 element in that the rates of convergence of the shear strains are in all cases quite close to 1.

CONCLUSIONS

Our objective in this paper was to briefly survey the theoretical formulation of our MITC plate bending elements and then, primarily, present some numerical convergence results.

The numerical results confirm to a high degree our theoretical results and show the effectiveness of the MITC elements. Of particular interest are the transverse shear stresses. A complete theoretical analysis for these stresses is not available yet, but we can firmly expect good behaviour, and the numerical results given in this paper confirm this expectation.

REFERENCES

1 Noor, A. *et al.* (Eds.) *Analytical and Computational Models of Shells*, CED-3, ASME Special Publication (1989)

2 Bathe, K. J. and Dvorkin, E. A formulation of general shell elements—the use of mixed interpolation of tensorial components, *Int. J. Num. Meth. Eng.*, **22**, 697–722 (1986)

3 Bathe, K. J. *Finite Element Procedures in Engineering Analysis*, Prentice-Hall, Englewood Cliffs, NJ (1982)

4 Bathe, K. J. and Ho, L. W. Some results in the analysis of thin shell structures, *Nonlinear Finite Element Analysis in Structural Mechanics* (Eds. W. Wunderlich, *et al.*), Springer-Verlag, Berlin, pp. 72–100 (1981)

5 Bathe, K. J. and Dvorkin, E. A four-node plate bending element based on Mindlin/Reissner plate theory and a mixed interpolation, *Int. J. Num. Meth. Eng.*, **21**, 367–383 (1985)

6 Dvorkin, E. and Bathe, K. J. A continuum mechanics based four-node shell element for general nonlinear analysis, *Eng. Comput.*, **1**, 77–88 (1984)

7 Bathe, K. J. and Brezzi, F. On the convergence of a four-node plate bending element based on Mindlin/Reissner plate theory and a mixed interpolation, *Proc. Conf. Math. Finite Elements Appl. V* (Ed. J. R. Whiteman), Academic Press, New York, pp. 491–503 (1985)

8 Bathe, K. J. and Brezzi, F. A simplified analysis of two plate bending elements—the MITC4 and MITC9 elements, in *Proc Int. Conf. Num. Meth. Eng. (NUMETA 87)* (Eds. G. N. Pande and J. Middleton), Martinus Nijhoff, Dordrecht, pp. D46 (1987)

9 Bathe, K. J., Brezzi, F. and Cho, S. W. The MITC7 and MITC9 plate bending elements, *Comput. Struct.*, **32**, 797–814 (1989)

10 Brezzi, F., Bathe, K. J. and Fortin, M. Mixed-interpolated elements for Reissner–Mindlin plates, *Int. J. Num. Meth. Eng.* **28**, 1787–1801 (1989)

11 Hinton, E. and Huang, H. C. A family of quadrilateral Mindlin plate elements with substitute shear strain fields, *Comput. Struct.* **23**, 409–431 (1986)

12 Brezzi, F., Fortin, M. and Stenberg, R. Error analysis for Reissner–Mindlin plate elements (to appear)

13 Brezzi, F. and Fortin, M., *Mixed and Hybrid Finite Element Methods*, Springer-Verlag (to appear)

14 Johnson, C. and Pitkäranta, J. Analysis of some mixed finite element methods related to reduced integration, *Math. Comp.*, **38**, 375–400 (1982)

15 Raviart, P. A. and Thomas, J. M. A mixed finite element method for second-order elliptic problems, *Mathematical Aspects of Finite Element Methods, Lecture Notes in Mathematics*, Vol. 606, Springer-Verlag, Berlin, pp. 292–315 (1975)

16 Sussman, T. and Bathe K. J. A finite element formulation for nonlinear incompressible elastic and inelastic analysis, *Comput. Struct.* **26**, 357–404 (1987)

17 Crouzeix, M. and Raviart, P. A. Conforming and nonconforming finite element methods for solving the stationary Stokes equations, *RAIRO Anal. Numer.* **R3**, 33–76 (1973)

18 Brezzi, F., Douglas, J., Jr., Fortin, M. and Marini, L. D. Efficient rectangular mixed finite elements in two and three space variables, *RAIRO, Math. Modell. Num. Anal.*, **21**, 581–604 (1987)

19 Arnold, D. N. and Falk, R. S. Edge effects in Reissner–Mindlin plate theory, in *Analytical and Computational Models of Shells*, CED-3 (Eds. A. K. Noor *et al.*), ASME Special Publication (1989)

20 Häggblad, B. and Bathe, K. J. Specifications of boundary conditions for Reissner–Mindlin plate bending finite elements, *Int. J. Num. Meth. Eng.*, **30**, 981–1011 (1990)